

Quantum random walks and wave-packet reshaping at the single-photon level

P. H. Souto Ribeiro,^{*} S. P. Walborn, C. Raitz, Jr., L. Davidovich, and N. Zagury

Instituto de Física, Universidade Federal do Rio de Janeiro, Caixa Postal 68528, Rio de Janeiro, RJ 21941-972, Brazil

(Received 22 February 2008; published 15 July 2008)

We realize an experimental implementation of one step of a quantum random walk at the single-photon level. After a single step, it is already possible to observe the difference between the quantum and classical random walk. The single photon is obtained using twin photons from parametric down-conversion, in which the detection of one photon of the idler prepares a single-photon state of the signal. We used two different experimental setups, one based on an interferometer and a second using a birefringent crystal. The physical process behind these effects is the spatial reshaping of the single-photon wave packet, which is the spatial analog of the time reshaping observed in tunneling experiments.

DOI: [10.1103/PhysRevA.78.012326](https://doi.org/10.1103/PhysRevA.78.012326)

PACS number(s): 42.50.Ex, 03.67.Ac, 42.25.Kb, 42.50.Ar

I. INTRODUCTION

In the simplest case of a classical random walk, a coin is tossed and, depending on the outcome, a walker makes one step to the left or to the right, each with 50% probability. After one iteration, the walker is $\pm \ell$ away from the initial position. This simple model has been proven to be very useful in the description of many physical processes. The quantum version of the random walk has been introduced by Aharonov, Davidovich, and Zagury [1], and the subject has been investigated by several authors [2–5]. Quantum random walks have been proposed as efficient subroutines for quantum-computing algorithms [2]. A quantum random walk works in much the same way as the classical case, with the difference characterized by the possibility of quantum interference between the probability amplitudes for the walker to make a step to the right and to the left. Because of interference, the displacement of a quantum walker can be very different from the classical case.

According to Ref. [1], the walker could be a quantum particle like an atom or a photon, and the coin might be an internal degree of freedom like the electronic spin or the photon polarization. Let us associate the position distribution of the walker with the photon configuration-space wave packet, and the coin with the polarization of the photon. In a step of the quantum walk algorithm, the photon undergoes some interaction depending on the polarization. For instance, in a birefringent crystal the photon wave packet is displaced (due to spatial walk-off) depending on its polarization state. If coherence is preserved, the total photon state evolves to an entangled state in which the configuration-space photon wave packet is entangled with polarization. An interesting consequence of this entanglement is that projection onto certain polarization states may cause the center of the photon wave packet to be strongly displaced [6]. This displacement can be much larger than the classical step [1]. Large displacements of the field amplitude distribution can also be obtained with classical waves, and this was indeed demonstrated experimentally with a laser [7]. In this context, the possibility of using classical-optics systems to simulate

quantum walks [4,5,8] and other results of quantum computation has been extensively discussed in the literature [9–16].

The physical process behind the difference between classical and quantum versions of the random walk is the reshaping of the photon wave packet. This is the spatial analog of the time reshaping that occurs in tunneling experiments [17,18], which investigate the tunneling of a single-photon wave packet through a one-dimensional photonic band-gap material. The results show a temporal displacement of the peak of the photon wave packet, as though it had traveled with a speed larger than c , the speed of light in vacuum. This effect was clearly explained in terms of the reshaping of the photon wave packet by interference. In the context of quantum mechanics, the reshaping involves the concept of weak measurement [19], also demonstrated with classical optics [7]. The relationship between photon tunneling and weak measurements was pointed out by Steinberg [17].

In this work we present an implementation of a one-step quantum walk at the *single*-photon level and observe the reshaping of the single-photon wave packet, which leads to an average displacement that can be much larger than the single classical step. In Sec. II we quickly review the theory. Detection of the idler photon in a twin-photon down-conversion process leads to the preparation of a one-photon state for the signal beam. This photon goes through either a Sagnac interferometer (Sec. III) or through a birefringent crystal (Sec. IV). Detection of the signal-photon polarization (the coin) in a convenient state leads to the reshaping of the photon wave packet and the large displacement of its center. We also point out, in Sec. V, the close connection between the reshaping of the photon wave packet in time and spatial domains. Finally we present our conclusions in Sec. VI.

II. THEORETICAL BACKGROUND

As mentioned before, the position distribution of the walker is associated with a single-photon configuration-space wave packet $\psi(x, y, z) = \langle x, y, z | \psi \rangle$, and the coin states $|V\rangle$ and $|H\rangle$ to the vertical and horizontal transverse linear polarizations states, respectively.

Let us assume that the photon is initially prepared in the state $|\Psi\rangle = |\psi\rangle|\text{coin}\rangle$ where $|\text{coin}\rangle = c_V|V\rangle + c_H|H\rangle$. Without loss of generality, c_V and c_H are taken to be real and positive.

^{*}phsr@if.ufrrj.br

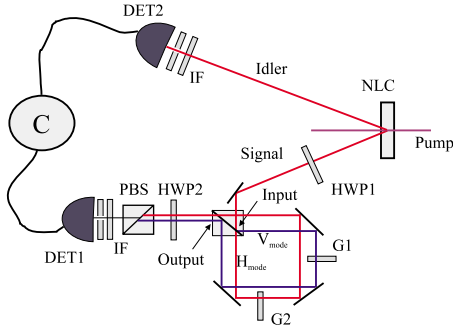


FIG. 1. (Color online) Sketch of the experiment with a Sagnac interferometer. NLC is nonlinear crystal, HWP1 and HWP2 are half-wave plates, G1 and G2 are glass plates, PBS is a polarizing beam splitter and IF means interference filter. There are detection apertures before detectors DET1 and DET2.

After one step $\pm \ell$ in the x direction, the quantum-walk algorithm transforms the initial state into an entangled state:

$$|\Psi\rangle \rightarrow c_V |\psi_\pm\rangle |V\rangle + c_H |\psi_\pm\rangle |H\rangle, \quad (1)$$

where $\langle x, y, z | \psi_\pm \rangle = \psi(x \pm \ell, y, z)$. The “flip of the coin” is implemented by projecting this state onto some polarization basis. For the linear polarization directions θ and $\theta + \pi/2$, the final wave packet of the walker is, respectively, and up to a normalization factor,

$$c_H \psi(x + \ell, y, z) + c_V (\tan \theta) \psi(x - \ell, y, z) \quad (2)$$

or

$$c_H (\tan \theta) \psi(x + \ell, y, z) - c_V \psi(x - \ell, y, z). \quad (3)$$

For an appropriate choice of θ , the position distribution of the walker and its average may be quite different from what we would expect classically. For example, if ℓ is much less than the width of the initial wave packet, and the result of the coin flipping is $\sin \theta |H\rangle - \cos \theta |V\rangle$, a displacement

$$\delta x = -\frac{c_V + c_H \tan \theta}{c_V - c_H \tan \theta} \ell \quad (4)$$

of the wave packet may occur with negligible deformation [1], as long as $|\delta x|$ is much smaller than the width of the initial wave packet. As pointed out in [1], by choosing $\tan \theta = (1 + \epsilon) c_V / c_H$, we obtain $\delta x \approx -2\ell / \epsilon$ if $|\epsilon| \ll 1$. Therefore it is possible to have $|\delta x| \gg \ell$. The probability of measuring the polarization at this angle θ depends on the initial state and decreases with ϵ .

III. EXPERIMENTAL REALIZATION WITH A SAGNAC INTERFEROMETER

The experimental setup is sketched in Fig. 1. A diode laser oscillating at 405 nm pumps a 5 mm thick lithium iodate nonlinear crystal. Type I spontaneous parametric down conversion (SPDC) produces vertically polarized signal and idler twin beams. The idler beam is sent through a 0.5 mm diameter pinhole and a 10 nm bandwidth interference filter centered around 810 nm, and is then detected. The signal

beam propagates through the half-wave plate HWP1 and is prepared in the initial state

$$|\Psi\rangle = |\psi\rangle (\alpha |V\rangle + \beta |H\rangle). \quad (5)$$

The amplitudes α and β , taken as real, satisfy $\alpha^2 + \beta^2 = 1$.

The signal photon goes through a Sagnac-like interferometer, which implements the coin tossing based on polarization. This interferometer is quite versatile and has been used to implement quantum channels in the investigation of the dynamics of entanglement [20]. The H component is transmitted through the input polarizing beam splitter (PBS), performing a round trip inside the interferometer in the counter-clockwise direction. The V component is reflected and performs a round trip in the opposite direction. Glass plates G1 and G2 are inserted in the paths of V and H modes, respectively, so that the optical path difference is kept balanced within the coherence length of the signal photon. By tilting one of these plates, it is possible to adjust the phase difference. To implement the polarization-dependent displacement of the photon path in the x direction, the H and V polarization paths inside the interferometer should not coincide. However, they are close enough to assure a high stability of the interferometer. Modes H and V are coherently recombined at the output beam splitter. For each arm of the interferometer, we define z as the propagation direction, x as the corresponding transverse direction on the plane of the interferometer, and y as the direction orthogonal to this plane (which corresponds to $y=0$). The alignment of the interferometer assures that H and V modes are recombined at the output with a small relative displacement. This implements one step of a polarization-dependent single-photon walk:

$$\begin{aligned} \psi(x, 0, z) (\alpha |V\rangle + \beta |H\rangle) \rightarrow & \alpha \psi(x - \ell, 0, z) |V\rangle \\ & + \beta \psi(x + \ell, 0, z) |H\rangle, \end{aligned} \quad (6)$$

where 2ℓ is the net separation between the centers of H and V wave packets in the direction x and is small in comparison to the transverse width of $\psi(x, 0, z) = \langle x, 0, z | \psi \rangle$, which is Gaussian in our experiment.

Detection of the transverse position of the signal photon is performed, after projection onto some linear polarization, implemented with the half-wave plate HWP2 and the polarizing beam splitter (PBS). Depending on this projection, different displacements of the center of the wave packet are possible. Projection onto H polarization results in a shift $-\ell$, while projection onto V polarization results in a shift ℓ , just like in the classical random walk. More interesting outcomes are obtained when the final state is projected onto a linear-polarization state corresponding to an angle θ in between H and V . Then the probability that the photon is detected in the position $(x, 0, z)$ is given by

$$P_\theta(x, 0, z) = N |\alpha \sin \theta \psi(x - \ell, 0, z) + \beta \cos \theta \psi(x + \ell, 0, z)|^2, \quad (7)$$

where N is a normalization factor. Notice that this projection results in interference between the wave packets associated with the H and V components of the state given in Eq. (7).

In our experiments, the quantum-correlated signal and idler beams are generated by an intense Gaussian pump

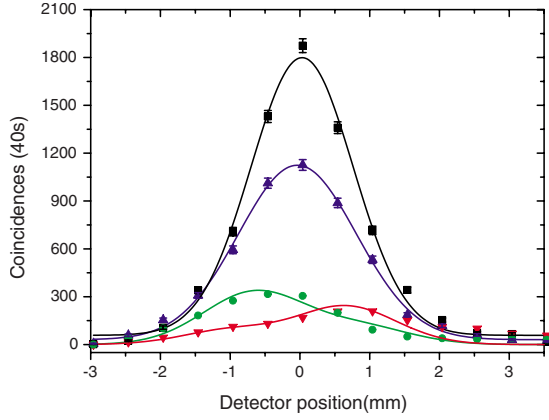


FIG. 2. (Color online) Experimental results for the interferometer setup. Black squares correspond to projection onto $V(\theta=90^\circ)$, blue up triangles to $H(\theta=0^\circ)$, red down triangles to $\theta=40^\circ$, and green circles to $\theta=50^\circ$. Solid lines are fittings to Gaussians for H and V and to Eq. (9) for $\theta=40^\circ$ and $\theta=50^\circ$. Error bars are obtained considering a Poissonian counting statistics. For the $\theta=40^\circ$ and $\theta=50^\circ$ curves, the error bars are smaller than the symbol.

beam; but the signal and idler beams, taken independently, do not propagate as Gaussian beams. However, as we perform coincidence detections in which the idler detector with a small pinhole acts as a trigger while the signal is scanned, the coincidence rate follows the pump beam Gaussian profile [22]. Therefore $\psi(x, 0, z)$ in Eq. (7) is given by

$$\psi(x, z) = \frac{A_0}{\sigma(z)} \exp\left[\frac{-x^2}{\sigma^2(z)}\right] \exp\left[-ikz - ik\frac{x^2}{2R(z)} + i\xi(z)\right], \quad (8)$$

where A_0 is a real normalization constant, $\sigma(z)$ is the beam width at propagation plane z , $R(z)$ is the radius of curvature of the wave front, and $\xi(z)$ is the Gouy phase [24]. Using Eq. (8) in Eq. (7), we obtain

$$P_\theta(x, z) = N \left(\frac{A_0}{\sigma(z)} \right)^2 \left\{ \alpha^2 \sin^2 \theta \exp\left[-2\frac{(x-l)^2}{\sigma_V^2(z)}\right] + \beta^2 \cos^2 \theta \exp\left[-2\frac{(x+l)^2}{\sigma_H^2(z)}\right] + 2 \cos(k_T x + \phi) \alpha \sin \theta \exp\left[-\frac{(x-l)^2}{\sigma_V^2(z)}\right] \times \beta \cos \theta \exp\left[-\frac{(x+l)^2}{\sigma_H^2(z)}\right] \right\}, \quad (9)$$

where $k_T = 2kl/R(z)$ and ϕ is the phase due to the optical path difference between H and V components. In principle $\sigma_V(z) = \sigma_H(z)$, however, in practice we have observed small differences between them, probably due to slightly different propagations of the H and V modes.

As it is seen in Eq. (9), the wave-front curvature is very important in the process because it gives rise to a phase modulation. We will use Eq. (9) to fit the interference curves.

Figure 2 shows the measured coincidence count rates

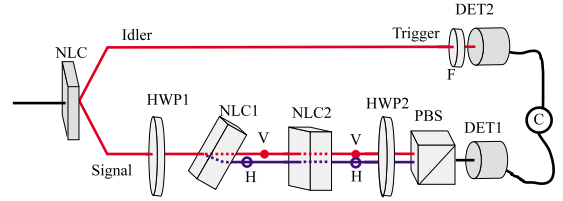


FIG. 3. (Color online) Sketch of the experiment with birefringent crystals. NLC means nonlinear crystal, HWP stands for half-wave-plate, PBS is a polarizing beam splitter, and F is a broadband infrared filter.

when the signal detector is scanned along the transverse x direction. Projections onto polarizations $H(0^\circ)$, $V(90^\circ)$, $\theta=40^\circ$, and $\theta=50^\circ$ are shown. All curves are initially fitted with Gaussians in order to determine the position of their peaks and the widths for H and V curves. From the Gaussian fits we obtain a classical step $\ell \approx 0.04$ mm and displacements $\delta x(50^\circ) \approx 0.7$ mm and $\delta x(40^\circ) \approx 0.4$ mm, corresponding to displacements of about $18 \times \ell$ and $10 \times \ell$, respectively. The direction of the displacement is determined by which one of the Gaussians dominates the interference. It is possible to control the displacement by adjusting the experimental parameters, so that $\alpha \sin \theta = (1 + \epsilon)\beta \cos \theta$, where ϵ is real and $|\epsilon| \ll 1$. The spatial phase modulation due to the wave-front curvature also influences the displacement, when the spatial frequency k_T is not small enough.

Finally, the curves were fitted with Eq. (9), using the amplitudes, peak position and widths of the H and V Gaussian fitted curves, and leaving k_T and ϕ as free parameters. The results were $k_T \approx 0.5$ mm $^{-1}$ and $\phi \approx 3.4$ rad for the adjusted polarization angle of $\theta=40^\circ$ and $k_T \approx 0.5$ mm $^{-1}$ and $\phi \approx 2.9$ rad for the adjusted polarization angle of $\theta=50^\circ$. The $\theta=40^\circ$ and $\theta=50^\circ$ curves are results of the interference between two propagating Gaussian wave packets. There is some disagreement between measurements and the fittings for these curves, in the region above 5.5 mm. This is probably due to background noise and in any case does not invalidate our conclusions.

IV. EXPERIMENTAL REALIZATION WITH BIREFRINGENT CRYSTALS

Figure 3 shows the experimental setup for the implementation of quantum random walk using a birefringent crystal. A He-Cd laser, oscillating at 442 nm, pumps a 5 mm long lithium iodate crystal. The pump laser is horizontally polarized and a type I SPDC interaction [23] takes place in the nonlinear crystal, so that vertically polarized photons are produced. The idler photon is sent directly to detection in a single-photon counting module (SPCM), through a broadband infrared filter. The detection wavelength is centered around 884 nm. The signal photon propagates through a half-wave plate (HWP), so that the coefficients α and β of its polarization state can be controlled, before it is sent to a 10 mm long lithium iodate birefringent crystal. The crystal is tilted, and because H and V polarizations experience different refractive indices, the refraction angles are different for each polarization. Therefore after the first crystal there is a

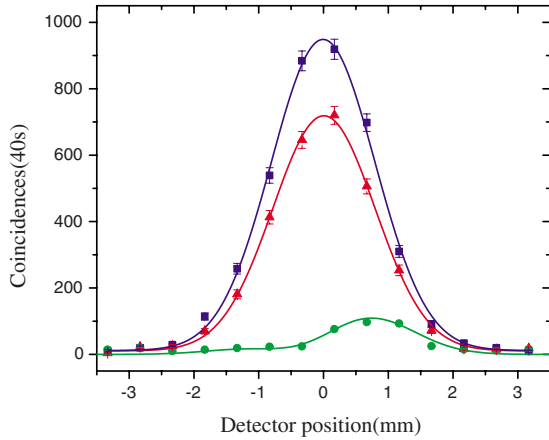


FIG. 4. (Color online) Experimental results for measurements with a birefringent crystal. Squares correspond to coincidences for projections onto $H(\theta=0^\circ)$, triangles correspond to $V(\theta=90^\circ)$, and circles correspond to 39° . Solid lines correspond to fittings to Gaussians for H and V curves and to Eq. (9) for $\theta=39^\circ$. Error bars are obtained considering a Poissonian counting statistics. For the $\theta=39^\circ$ curve, the error bars are smaller than the symbol.

vertical shift and the propagation path followed by mode H is slightly higher than V . In practice, care must be taken in order to preserve the coherence between H and V components. Propagation through the birefringent crystal also separates the wave packets in the longitudinal direction, making them temporally distinguishable. We compensate this separation using a second crystal of the same length and its optical axis rotated 90° with respect to the first one. In this way it is possible to compensate the longitudinal separation preserving the transverse separation between H and V components. After propagation through the second crystal, the photon is sent to a polarization analyzer and detector. A SPCM detector is used, with a 10 nm bandwidth interference filter, centered around 884 nm.

Figure 4 shows the measured coincidence count rates when the signal detector is scanned along the vertical direction. Projections onto polarizations $H(\theta=0^\circ)$, $V(\theta=90^\circ)$, and $\theta=39^\circ$ are shown. The projections are implemented with HWP2 and PBS. All experimental curves are initially fitted with Gaussian functions. The separation between the peaks of the distributions for H and V is $2\ell \approx 0.01$ mm, while the peak of distribution obtained for $\theta=39^\circ$ is displaced by $\delta x \approx 0.7$ mm from the mean position between H and V . The interference curve is then fitted with Eq. (9), using the amplitudes, peak position, and widths of the H and V Gaussian fitted curves, and leaving k_T and ϕ as free parameters. The results were $k_T \approx 0.45$ mm $^{-1}$ and $\phi \approx 3.4$ rad for the adjusted polarization angle of $\theta=39^\circ$. The results are in good agreement with the measurements.

In this case it is worth noting that this remarkable relative displacement of about 140 times the classical step size would not be observable without the spatial phase modulation due to the wave-front curvature. The increase in the coincidence count rate in the region of the peak of the reshaped wave packet is due to this modulation. In other words, if the same experiment were realized using a wave front with $k_T \rightarrow 0$, the probability of detecting a photon with such a large displace-

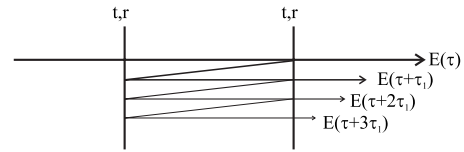


FIG. 5. Propagation through a Fabry-Perot interferometer.

ment would be extremely small. Similar effects have recently been observed in the context of weak measurements [21]. If it is convenient, the wave-front curvature can be controlled through the pump beam, in the case of our setup with twin photons [22].

V. ANALOGY WITH RESHAPING IN TIME

Displacements larger than the step size are a consequence of the interference process, which reshapes the single-photon wave packet in an analogous fashion as in photon tunneling experiments [17,18]. In order to demonstrate this, let us consider the propagation of a photon wave packet through a Fabry-Perot interferometer in the time domain, as sketched in Fig. 5. Suppose that the input and output mirrors have the same amplitude transmission t and reflection r coefficients. The output field has a contribution that comes from the transmitted component of the wave packet given by $t^2 E(\tau)$ and contributions coming from one round trip, corresponding to internal reflection and subsequent transmission given by $t^2 r^2 e^{i\phi} E(\tau_1)$, where ϕ is the phase and τ_1 is the time delay accumulated after one roundtrip, and so on. Therefore the output field is given by $E_T = t^2 [E(\tau) + r^2 e^{i\phi} E(\tau + \tau_1) + r^4 e^{2i\phi} E(\tau + 2\tau_1) + \dots]$.

The resulting interference is illustrated in Fig. 6. The larger Gaussian corresponds to the direct transmission component of the wave packet. Its peak gives the time reference which is the same as if the wave packet would have propagated without the cavity. The smaller Gaussian is the result of the interference between the transmission components, calculated keeping terms up to r^4 . Time is in arbitrary units

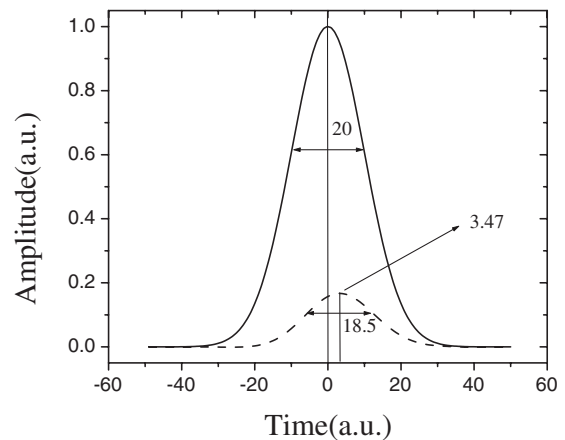


FIG. 6. Temporal reshaping of the wave packet in a Fabry-Perot interferometer. The solid line corresponds to the amplitude of the directly transmitted wave packet and the dashed line corresponds to the wave packet reshaped by interference.

(a.u.). It is seen that for $r=0.99$, $t=0.14$, and $\phi=\pi$, the transmitted field is a Gaussian displaced 3.47 a.u. toward the future, given that the input wave packet has a width of 20 a.u. The reshaping of the wave packet produces, in this case, the counterintuitive effect of displacement to the future. While for this system the displacement results from interference between many wave packets, in the spatial case the same effect results from interference between only two wave packets and thus leads to a simple understanding of the underlying physical process. In addition, it is very easy to measure the corresponding spatial displacement, while in the time domain a Hong-Ou-Mandel interferometer [25] is required for high-precision measurement of temporal displacements of single photons.

VI. CONCLUSIONS

One step of a quantum random walk is implemented at the single-photon level. The walker is associated with the photon

transverse spatial distribution, while the coin is represented by the polarization. Even after only one step, it is possible to observe the difference between the classical and the quantum walk. Projection onto certain polarization states results in a large interference of the two spatial components of the photon state. As a consequence, the “walker” makes a step much larger than the classical step. It is possible to extend the walk to a larger number of iterations. Our experiment may be considered as the spatial analog of photon tunneling in the time domain. However, here the reshaping of the photon wave packet results in a spatial rather than a temporal displacement.

ACKNOWLEDGMENTS

The authors acknowledge financial support from the Brazilian funding agencies CNPq, CAPES, PRONEX, and FAPERJ. This work was performed as part of the Brazilian Millennium Institute for Quantum Information.

-
- [1] Y. Aharonov, L. Davidovich, and N. Zagury, *Phys. Rev. A* **48**, 1687 (1993).
- [2] J. Kempe, *Contemp. Phys.* **44**, 307 (2003).
- [3] P. K. Pathak and G. S. Agarwal, *Phys. Rev. A* **75**, 032351 (2007).
- [4] B. Do, M. L. Stohler, S. Balasubramanian, D. S. Elliott, C. Eash, E. Fischbach, M. A. Fischbach, A. Mills, and B. Zwickl, *J. Opt. Soc. Am. B* **22**, 499 (2005).
- [5] P. L. Knight, E. Roldan, and J. E. Sipe, *Phys. Rev. A* **68**, 020301(R) (2003).
- [6] The possibility of attributing an approximate position to a photon in the optical regime was demonstrated by L. Mandel, *Phys. Rev.* **144**, 1071 (1966).
- [7] N. W. M. Ritchie, J. G. Story, and G. Randall Hulet, *Phys. Rev. Lett.* **66**, 1107 (1991).
- [8] D. Francisco, C. Iemmi, J. P. Paz, and S. Ledesma, *Phys. Rev. A* **74**, 052327 (2006).
- [9] N. J. Cerf, C. Adami, and P. G. Kwiat, *Phys. Rev. A* **57**, R1477 (1998).
- [10] P. Kwait, J. Mitchell, P. Schwindt, and A. White, *J. Mod. Opt.* **47**, 257 (2000).
- [11] R. J. C. Spreeuw, *Found. Phys.* **28**, 361 (1998); *Phys. Rev. A* **63**, 062302 (2001).
- [12] N. Bhattacharya, H. B. van Linden van den Heuvell, and R. J. C. Spreeuw, *Phys. Rev. Lett.* **88**, 137901 (2002).
- [13] G. Puentes, C. La Mela, S. Ledesma, C. Iemmi, J. P. Paz, and M. Saraceno, *Phys. Rev. A* **69**, 042319 (2004).
- [14] H. Jeong, M. Paternostro, and M. S. Kim, *Phys. Rev. A* **69**, 012310 (2004).
- [15] A. N. Oliveira, S. P. Walborn, and C. H. Monken, *J. Opt. B: Quantum Semiclassical Opt.* **7**, 288 (2005).
- [16] D. Francisco, C. Iemmi, J. P. Paz, and S. Ledesma, *Opt. Commun.* **268**, 340 (2006).
- [17] A. M. Steinberg, *Phys. Rev. A* **52**, 32 (1995).
- [18] A. M. Steinberg, P. G. Kwiat, and R. Y. Chiao, *Phys. Rev. Lett.* **71**, 708 (1993).
- [19] Y. Aharonov, D. Z. Albert, and L. Vaidman, *Phys. Rev. Lett.* **60**, 1351 (1988).
- [20] M. P. Almeida, F. de Melo, M. Hor-Meyll, A. Salles, S. P. Walborn, P. H. Souto Ribeiro, and L. Davidovich, *Science* **316**, 579 (2007).
- [21] O. Hosten and P. G. Kwiat, *Science* **319**, 787 (2008).
- [22] C. H. Monken, P. H. Souto Ribeiro, and S. Pádua, *Phys. Rev. A* **57**, 3123 (1998).
- [23] See, for instance, A. Yariv, *Quantum Electronics* (Wiley, New York, 1967), Chap. 21.
- [24] See, for instance, Bahaa E. A. Saleh and Malvin Carl Teich, *Fundamentals of Photonics* (Wiley, New York, 1991), Chap. 3, pp. 80–107.
- [25] C. K. Hong, Z. Y. Ou, and L. Mandel, *Phys. Rev. Lett.* **59**, 2044 (1987).